Accepted Manuscript

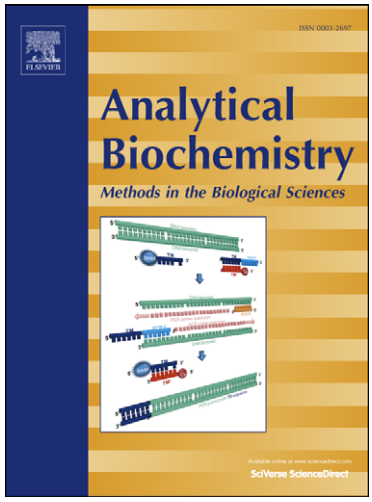

An acetylcholinesterase biosensor based on platinum nanoparticles-carboxylic graphene-nafion modified electrode for detection of pesticides

Long Yang, Guangcan Wang, Yongjun Liu

PII: S0003-2697(13)00123-1
DOI: http://dx.doi.org/10.1016/j.ab.2013.03.004
Reference: YABIO 11277

To appear in: *Analytical Biochemistry*

Received Date: 16 December 2012
Revised Date: 2 March 2013
Accepted Date: 4 March 2013

Please cite this article as: L. Yang, G. Wang, Y. Liu, An acetylcholinesterase biosensor based on platinum nanoparticles-carboxylic graphene-nafion modified electrode for detection of pesticides, *Analytical Biochemistry* (2013), doi: http://dx.doi.org/10.1016/j.ab.2013.03.004

This is a PDF file of an unedited manuscript that has been accepted for publication. As a service to our customers we are providing this early version of the manuscript. The manuscript will undergo copyediting, typesetting, and review of the resulting proof before it is published in its final form. Please note that during the production process errors may be discovered which could affect the content, and all legal disclaimers that apply to the journal pertain.

ACCEPTED MANUSCRIPT

Title page:

Title: An acetylcholinesterase biosensor based on platinum nanoparticles-carboxylic graphene-nafion modified electrode for detection of pesticides

Short title: AChE biosensor based on Pt NPs-CGR-NF/GCE

Subject category: enzymatic assays and analyses

Long Yang, Guangcan Wang*, Yongjun Liu

School of Chemical Science and engineering, Yunnan University, Kunming 650091, China

**Corresponding author: Guangcan Wang, E-mail address: wangc166163@sina.com*

Tel: 86-871-5033218, Fax: 86-871-5033214

ACCEPTED MANUSCRIPT

ACCEPTED MANUSCRIPT

Abstract: A sensitive amperometric acetylcholinesterase (AChE) biosensor based on platinum nanoparticles (Pt NPs), carboxylic graphene (CGR) and nafion (NF) modified glassy carbon electrode (GCE) has been developed. The Pt NPs-CGR-NF nanocomposites with excellent conductivity, catalysis and biocompatibility offered an extremely hydrophilic surface for AChE adhesion. Chitosan (CS) was used as cross-linker to immobilize the AChE on Pt-CGR-NF modified GCE. NF was used as a protective membrane of the AChE biosensors. The AChE biosensor showed favorable affinity to acetylthiocholine chloride (ATCl) and could catalyze the hydrolysis of ATCl with an apparent Michaelis–Menten constant value of 148 μM. Under optimum conditions, the biosensor detected methyl parathion in the linear range from 1.0×10^{-13} to 1×10^{-10}M and from 1.0×10^{-10} to 1×10^{-8}M with the detection limit of 5×10^{-14}M and detected carbofuran in the linear range from 1.0×10^{-12} to 1×10^{-10}M and from 1.0×10^{-10} to 1×10^{-8}M with the detection limit of 5×10^{-13}M. The biosensor exhibited good sensitivity, acceptable stability and reproducibility, thus providing a promising tool for analysis of enzyme inhibitors.

Keywords*:* carboxylic graphene; platinum nanoparticles; acetylcholinesterase; amperometric biosensor; stability

Introduction

A great number of pesticides are commonly and widely used to raise crop productivity and attracted attention of legislators and scientists [1]. The pesticides persistence in the environment and their presence in water and food posses a very potential hazard to human health because they irreversibly inhibit the catalytic active sites of acetylcholinesterase (AChE)[1], an essential enzyme of the central nervous system (CNS) of mammals; AChE catalyses the hydrolysis of acetylcholine which is a neurotransmitter in the CNS [2]. In recent years, biosensors based on AChE have emerged as a promising technique for toxicity analysis, environmental monitoring, food quality control and military investigations [3, 4]. The main application of AChE biosensors is for the detection of organophosphate and carbamate pesticides based on enzyme inhibition. These devices are designed to complement or replace the existing reference analytical methods such as HPLC and GC/MS by simplifying or eliminating sample preparation, thus decreasing the analysis time and cost.

ACCEPTED MANUSCRIPT

Graphene, a two-dimensional sheet of sp^2-bonded carbon atoms arranged in a honeycomb lattice, has attracted increasing attention since it was first isolated from three-dimensional graphite by mechanical exfoliation [5]. Due to its extraordinary thermal, mechanical, and electrical properties, graphene is usually considered as a competitive candidate for next-generation electronic applications such as electronic and energy storage devices such as supercapacitors [6, 7], batteries [8, 9], fuel cells [10,11], solar cells [12, 13], sensors [14, 15], biosensors [16, 17], catalysts [18, 19], etc. However, many researches have reported that the pure graphene actually exhibit unsatisfactory electrical conductivity because of the inevitable aggregation [20, 21]. Some of the useful and unique properties of graphene can only be realized after it is functionalized with organic groups such as hydroxyl, carboxyl, amino and the like [22, 23]. A useful method to prepare functionalized graphene is incorporated into chemical functional groups by covalent bonding on the graphene sheets. Functionalized graphene sheets are easier to disperse in organic solvents, which can improve the dispersion and homogeneity of the graphene within the polymer and yield novel types of electrically conductive nanocomposites [20, 21].

Noble metal nanoparticles and graphene nanohybrids are an important kind of nanocomposite materials which successfully integrate the unique properties of two class materials and exhibit some new functions caused by the cooperative effects between the noble metal nanoparticles and graphene such as excellent electron mobility, catalytic activity and so on. Among these nanocomposites, noble metal nanoparticles are usually anchored on the surface of these two-dimensional supports of graphene sheets [24, 25]. The existing research results indicated that noble metal nanoparticles and graphene nanohybrids modified GCE showed high electron mobility, catalytic activity and sensitivity [26-28]. However, many of the interesting and unique properties of the nanocomposite can only be realized after it is integrated into more complex assemblies [20, 21]. We were particularly interested in Pt, because Pt/graphene with excellent conductivity has attracted a great deal of attention as a good catalyst. CGR with carboxyl functional group could be bounded with Pt NPs. The cooperative effects between the Pt NPs and CGR might enhance the performance of the Pt NPs-CGR nanocomposite. Pt NPs could be separated and formed uniform Pt NPs on functionalized graphene sheets. According to these existing researches, we developed the AChE biosensor based on Pt NPs-CGR-NF nanocomposite.

In this work, CGR and Pt NPs-CGR nanocpmposites have been synthesized by chemical method

ACCEPTED MANUSCRIPT

and characterized by electron microscopy (SEM), fourier transform infrared spectra (FTIR) and UV-vis absorption spectroscopy (UV-vis). The synthesized PtNPs-CGR nanocomposites are easily dispersed in NF solution. The Pt NPs-CGR-NF film with excellent conductivity, catalysis and biocompatibility offered a hydrophilic surface for biomolecule adhesion. CS was used as cross-linker to immobilize the AChE on PtNPs-CGR-NF modified GCE. NF was used as a protective membrane of the AChE biosensors. The NF/AChE-CS/PtNPs-CGR-NF/GCE biosensor might be an effective device for detection of pesticides.

Experimental

Reagents and Apparatus

ATCl, AChE (Type C3389, 500 U/mg from electric eel), CS (85% deacetylation), NF (5% in lower aliphatic alcohols and water) were purchased from Sigma–Aldrich (St. Louis, USA). Methyl parathion and carbofuran (99.99%) was obtained from Institution of environmental protection of China's Agriculture Ministry (Beijing China). Graphite powder was purchased from Sinopharm Chemical Reageat Company. (China). $H_2PtCl_6{\cdot}6H_2O$ was obtained from Shanghai Chemical Reagent Co. Ltd. (China). All other reagents were of analytical grade. Aqueous solutions were prepared with deionized (DI) water (18 MΩ cm).

The electrochemical measurements were carried out on an IM6ex electrochemical workstation (Zahner Elektrik Instruments, Germany). A conventional three-electrode system was employed with a saturated calomel electrode (SCE) as the reference electrode, a platinum foil as the counter electrode, and the modified GCE (diameter＝3mm) as the working electrodes. Cyclic voltammetry (CV) measurements were performed in 0.1M phosphate buffer solution (PBS, pH 7.4). All experiments were performed at room temperature (25±1℃). CGR and Pt NPs-CGR nanocomposites were characterized by scanning electron microscopy (SEM, QUNT200 USA), fourier transform infrared spectrometry (FTIR, Thermo Fisher SCIENTIFIC Nicolet IS10 USA) and UV–vis absorption spectroscopy (UV–vis, HITACHI U-4100 Japan).

Preparation of CGR

ACCEPTED MANUSCRIPT

Graphite oxide prepared by Hummer's Method [29] was suspended in water and exfoliated through ultrasonication (2 h) to obtain graphene oxide (GO) solution. GO solution was centrifuged at 3000 rpm to remove unexfoliated graphite oxide. CGR was prepared by a chemical method. Briefly, GO aqueous suspension (5mL) was diluted as to give a concentration of 2.0mg/mL, and then sonicated for 1 h to give a clear solution. 1.2g of NaOH and 1.0g chloroacetic acid (Cl-CH_2-COOH) were added to the suspension and sonicated for 3 h to convert the -OH groups to -COOH via conjugation of acetic acid moieties. Sequentially the suspension was separated by centrifuging at a speed of 15,000 rpm, washed with DI water for several cycles, dried in an oven at 50℃ to gain CGR [30].

Synthesis Pt NPs-CGR nanocomposites

The Pt-CGR NPs were prepared as follows: briefly, 2.0mg CGR were suspended in 100μl of 0.01M $H_2PtCl_6 \cdot 6H_2O$ by sonicating for 10 min to disperse CGR equably. Then 100μl of 0.01M sodium citrate, 10.0ml ethanol and 20.0ml DI water were added to the above suspension. Ice-cold, freshly prepared 120μl of 0.05 M $NaBH_4$ solution was added to the above mixture while stirring until the color of the solution did not change. After stirring for an additional 10 h, the brown suspending liquid was separated by centrifuging at a speed of 16,000 rpm, washed with DI water for several cycles, dried in an oven at 60℃, and then stored in a brown bottle at 4℃[31, 32].

Preparation of AChE biosensor

NF solution (0.125%, W_t/V) was prepared by diluting 5% of NF with ethanol and DI water (V/V, 1/1). 0.5mg of the Pt NPs-CGR was added to 1.0 ml of the NF solution before sonication to produce a homogeneous suspension of Pt NPs-CGR-NF. Similarly, 0.5mg/ml of CGR-NF and 0.5mg/ml of GO-NF homogeneous suspension were prepared in the same way. The suspensions were stored at 4°C.

The Pt NPs-CGR-NF/GCE was produced by casting 5μl of the 0.5mg/ml Pt NPs-CGR-NF suspension onto the GCE and drying at room temperature. A similar casting procedure was used to produce CGR-NF/GCE and GO-NF/GCE. The enzyme solution was mixed as 0.05U AChE and 0.2% CS (W_t/V, 50 mM acetic acids). The modified electrodes were each coated 4.5μl of AChE-CS (V/V,

ACCEPTED MANUSCRIPT

2/1) and dried overnight at 4℃. The AChE-CS/PtNPs-CGR-NF/GCE, AChE-CS/CGR-NF/GCE and AChE-CS/GO-NF/GCE biosensors were obtained and washed with 0.1M PBS to remove the unbound AChE. Finally, three types of biosensor were covered with 3μl 0.1% (W_t/V) NF as a protective membrane and then stored at 4℃. Thus, three types of biosensor structure were: NF/AChE-CS/PtNPs-CGR-NF/GCE, NF/AChE-CS/CGR-NF/GCE and NF/AChE-CS/GO-NF/GCE. NF/AChE-CS/GCE was also produced as a control.

Results and discussion

Characterization of Pt NPs-CGR nanocomposites

The SEM image in Fig. 1 (a) showed a typical wrinkled sheet texture of GO. Fig. 1 (b) illustrated the typical SEM image of the prepared CGR sheets. As shown in this figure, CGR clearly showed the flake-like shapes. Fig. 1 (c) showed the typical SEM image of the synthesized Pt NPs-CGR, which demonstrated that the CGR could be uniformly covered with Pt NPs.

In Fig. 2A, the FTIR spectrum of GO (curve a) displayed the presence of -OH (3413 cm^{-1}), C=O (1731 cm^{-1}), C=C (1621 cm^{-1}) and C–O (1047 cm^{-1}), ascribed to the stretching vibrations of GO. FTIR results for the CGR are shown in Fig. 2A (curve b). The appearance of strong peaks at 3424cm^{-1} and 1727cm^{-1} confirmed the presence of the carboxylic group. The absorption peaks at 2352 and 1223 cm^{-1} disappeared for CGR, which indicated that there may be a bit of impurities in GO samples. The higher ratio of the magnitude of the peaks ascribed to C=O in CGR indicated that the peaks ascribed to C=O was enhanced after carboxyl functionalized.

The amount of Pt NPs synthesized on the surface of CGR was investigated by using UV-vis. Fig. 2B showws absorption spectra of Pt NPs synthesized in the absence of CGR (curve a) and in the presence of CGR (curve b), respectively. Both Pt NPs and Pt NPs-CGR nanocomposites displayed an absorption band at 216nm, which was a characteristic peak of well-dispersed Pt NPs. These results demonstrated that Pt NPs have been efficiently deposited onto the CGR surface without aggregation. From the loss of intensity at 216nm, 96% Pt NPs was deposited on the CGR roughly.

Electrochemical behavior of the biosensors

ACCEPTED MANUSCRIPT

CV of ATCl and enzymatic product thiocholine was investigated on four different biosensors as shown in Fig. 3A. No amperometric response could be observed at NF/AChE-CS/NF/GCE (curve a), NF/AChE-CS/GO-NF/GCE (curve b), NF/AChE-CS/CGR-NF/GCE (curve c), and NF/AChE-CS/Pt NPs-CGR-NF/GCE (curve d) in PBS (pH 7.4). However, when 0.5mM ATCl was added into the detection PBS (pH 7.4), an obvious amperometric response was observed at NF/AChE-CS/NF/GCE (curve e), NF/AChE-CS/GO-NF/GCE (curve f), NF/AChE-CS/CGR-NF/GCE (curve g) and NF/AChE-CS/PtNPs-CGR-NF/GCE (curve h). Obviously, these amperometric responses were attributed to the oxidation of thiocholine produced by the hydrolysis of ATCl, which were catalyzed by immobilized AChE. Fig. 3A showed the oxidation peak currents increased and the oxidation peak potentials shift negatively in sequence. At NF/AChE-CS/Pt NPs-CGR-NF/GCE, the oxidation peak current was the highest and peak potential was the lowest in three biosensors (curve h). It indicated Pt NPs-CGR could greatly improve electron transfer which increases peak current and sensitivity of the biosensor. Meanwhile, Pt NPs-CGR could enhance catalysis to decrease the potential which was beneficial for avoiding interference from other electroactive species in biological matrix. The amperometric response in the case of CGR-NF was at an 80% level of that for Pt NPs-CGR-NF, which indicated that Pt NPs could enhance the sensitivity of the biosensor in the detection of pesticides. Pt NPs-CGR-NF nanocomposite modified electrodes possessing good conductivity and catalytic activity provided an extremely hydrophilic surface for AChE adhesion. Using CS immobilization AChE on the surface of Pt NPs-CGR-NF/GCE could keep high enzyme activity and improve electron transmission between the enzyme and the modified electrode. Finally, NF film was used to prevent the loss of the enzyme molecules, improve the anti-interference ability of the biosensor and provide a biocompatible microenvironment to maintain enzymatic activity.

Optimization of the preparation of the biosensor

The effect of the dosage of Pt NPs-CGR-NF on amperometric response of the AChE-CS/Pt NPs-CGR-NF/GCE biosensor was studied as shown in Fig. S1. During the dosage of Pt NPs-CGR-NF ranged from 3 to 9μl, the amperometric response increased along with the modified dosage. When the dosage exceeded 5μl, the amperometric response did not significantly increase and the base line turned high, possibly because of increased resistance and double layer capacitance of the modified electrode.

ACCEPTED MANUSCRIPT

Hence, the optimal dosage of Pt NPs-CGR-NF was 5μl.

The amperometric response of the biosensor to ATCl was also affected by the ratio of Pt NPs in Pt NPs-CGR as shown in Fig. S2. When the ratio of Pt NPs was from 3 w_t% to 8 w_t%, the amperometric response increased with the ratio of Pt NPs. As the ratio of Pt NPs exceeded 5 w_t%, amperometric response did not significantly increase and the base line turned high, possibly because of Pt NPs aggregation and not well separated at CGR. Then, the optimal ratio was selected as 5 w_t%.

The amount of enzyme immobilized on the electrode surface was another important aspect of the preparation as shown in Fig. S3. Fewer of AChE did not hydrolyze and catalyze ATCl completely. With increasing of AChE, the amperometric response increased and reached at the maximum of 0.15U. Further increasing of AChE led to an obvious decrease of the amperometric response. Therefore, superabundant AChE possibly increased resistance of the modified electrode and was unstable. Thus, 0.15U of AChE was used in these experiments.

In order to enhance the stability of the biosensor, CS was used as cross-linker to immobilize the AChE on Pt NPs-CGR-NF/GCE and improve electronic transmission between AChE and Pt NPs-CGR-NF/GCE. NF was used as the protective membrane for the AChE biosensor. The NF/AChE-CS/PtNPs-CGR-NF/GCE, AChE-CS/PtNPs-CGR-NF/GCE and AChE/PtNPs-CGR-NF/GCE biosensors were continuously tested 6 times respectively in PBS (pH7.4) containing 0.5mM ATCl solution (Fig. 3B). These RSD of amperometric response of the three above biosensors were 2.16% (a), 7.49% (b), 14.33% (c), respectively. The results showed that the CS as cross-linker immobilized AChE and the NF protective membrane effectively improved stability of the AChE biosensor.

The bioactivity of the immobilized AChE depends on the pH of the ATCl solution. The relationship between amperometric responses of AChE with the pH of the ATCl solution was showed in Fig. S4. In the pH range from 6.8 to 8.0, the amperometric response increases with increasing pH and reached a maximum at 7.4. The farther increase of the pH leads to an obvious decrease of the amperometric response. Therefore, pH 7.4 was used in the detection solution.

Detection of ATCl

The AChE biosensor was explored by CV measurements according to the above optimum conditions. Fig. 4A showed the amperometric response at the NF/AChE-CS/Pt NPs-CGR-NF/GCE at

ACCEPTED MANUSCRIPT

0.50V in a stirred solution, which was added an ATCl stock solution. With increasing ATCl concentration, the amperometric response of the biosensor increases. The amperometric response of the biosensor was a linear function of ATCl concentration in two segments. One was from 0.2μM to 20μM; the other was from 20μM to 500μM. The detection limit was 0.1μM. At higher ATCl concentrations, the shape of the amperometric response was indicative of a Michaelis–Menten process (Fig. 4B). The inflection point indicated that the linear range of AChE biosensors for acetylcholine was approximately two orders of magnitude. When the concentration of ATCl was saturated, the amperometric response gradually tended to a constant value. The apparent Michaelis-Menten constant (κ_m^{app}) in the present studies was calculated to be 148 μM according to Lineweaver-Burk equation. This value was lower than that for AChE immobilized on 3-carboxyphenylboronic acid/reduced graphene oxide-gold nanocomposites modified electrode (0.16mM) [33], for AChE immobilized on CdS-decorated graphene nanocomposite modified electrode (0.24mM) [34], for AChE immobilized on improved hydrophobic gold nanoparticle/prussian blue modified electrode (0.3mM) [35] and for AChE immobilized on liposome bioreactors-chitosan nanocomposite film (0.36mM) [36], indicating that the AChE biosensor had a great affinity and catalysis to its substrate ATCl.

Effect of incubation time

It is recognized that pesticides have the same general structure and toxicological mode of action. In this work, methyl parathion was used as a model pesticide. The residual activity of the enzyme was influenced by the exposure time of the AChE to methyl parathion. The exposure time was controlled by incubation time of AChE with inhibitor. As shown in Fig. S5, the inhibition of enzyme increases with increasing incubation time. 6-min exposure time was chosen as the best compromise between exposure time and sensitivity.

Detection of the pesticides

After incubation of the biosensor with different concentration methyl parathion, respectively, amperometric responses of the biosensor were determined, respectively, as shown in Fig. 5A. It showed that methyl parathion reduces the activity of the immobilized AChE. Fig. 5B showed the

ACCEPTED MANUSCRIPT

calibration plots of methyl parathion and carbofuran. Linear equations of methyl parathion were I(%)=8.35lgC+133.91 (r=0.997) from 10^{-13} to 10^{-10}M and I(%)=2.73lgC+77.07 (r=0.998) from 10^{-10} to 10^{-8}M. Linear equations of carbofuran were I(%)=11.97gC+170.95 (r=0.998) from 10^{-12} to 10^{-10}M and I(%)=3.23lgC+83.21 (r=0.998) from 10^{-10} to 10^{-8}M. The detection limits of methyl parathion and carbofuran were 5×10^{-14}M 5×10^{-13}M, respectively. The inflection point indicated that the biosensor was more sensitive for detecting low concentration of pesticides than high concentration of pesticides. The performances of the biosensor compared with those reported in literature were summarized in Table1.

Interference study

The interfering signal due to the most common electroactive species was studied. The signal for a 0.5mM ATCl was compared with the signal obtained in the presence of the interfering species. The test result showed no noticeable changes in amperometric response were detected in the presence of glucose (0.5mM), citric acid (0.5mM) and oxalic acid (0.5mM) respectively at the present operating potential in this system. However, 0.5mM of p-nitrophenol severely interfered with the determination. Besides, equal concentration of methyl parathion and carbofuran severely interfered with each other for the determination.

Precision of measurements and stability of biosensor

The intra-assay precision of the biosensor was evaluated by testing one NF/AChE-CS/PtNPs-CGR-CS/GCE for six times in 0.5mM ATCl after being immersed in the 1.0×10^{-10} M methyl parathion for 6-min. The inter-assay precision was estimated with six different biosensors in the same way. The two RSD of intra-assay and inter-assay were found to be 3.8% and 6.2%, respectively, indicating an acceptable reproducibility. When the enzyme electrode was not in use, it was stored at 4℃ in dry condition. No obvious decrease in the response of ATCl was observed in the first 10-day storage. After a 30-day storage period, the sensor retained 90% of its initial amperometric response, indicating the acceptable stability of biosensor.

Conclusion

ACCEPTED MANUSCRIPT

The AChE biosensor based on Pt NPs-CGR-NF has been developed. Stability of the AChE biosensor was improved by using CS as cross-linker to immobilize the AChE on the Pt NPs-CGR-NF/GCE and NF as a protective membrane of the biosensor. The biosensor showed low applied potential, good fabrication reproducibility, acceptable stability, fast response and low detection limit. The method might be extended to assemble other biological molecules, such as antibody, antigen and DNA for wide bioassay applications.

ACCEPTED MANUSCRIPT

ACCEPTED MANUSCRIPT

References:

[1] G.L. Turdean, M.S. Turdean, Synergetic effect of organic solvents and paraoxon on the immobilized acetylcholinesterase, Pestic. Biochem. Physiol. 90 (2008) 73-81.

[2] J. Miroslaw, S.G.M. Smogorzewski, Altered Acetylcholine Metabolism of Brain in Uremia: Role of Secondary Hyperparathyroidism, J. Renal Nutr. 18 (2008) 122-126.

[3] S. Andreescu, J.L. Marty, Twenty years research in cholinesterase biosensors: From basic research to practical applications, Biomol. Eng. 23 (2006) 1-15.

[4] R. Rawal, S. Chawla, T. Dahiya, C.S. Pundir, Development of an amperometric sulfite biosensor based on a gold nanoparticles/chitosan/multiwalled carbon nanotubes/polyaniline-modified gold electrode, Anal. Bioanal. Chem. 401 (2011) 2599-2608.

[5] K.S. Novoselov, A.K. Geim, S.V. Morozov, D. Jiang, Y. Zhang, S.V. Dubonos, I.V. Grigorieva and A.A. Firsov, Electric Field Effect in Atomically Thin Carbon Films, Science 306 (2004) 666-669.

[6] M.D. Stoller, S.J. Park, Y.W. Zhu, J.H. An, R.S. Ruoff, Graphene-Based Ultracapacitors, Nano Lett. 8 (2008) 3498-3502.

[7] A.K. Mishra, S. Ramaprabhu, Functionalized Graphene-Based Nanocomposites for Supercapacitor Application, J. Phys. Chem. C 115 (2011) 14006-14013.

[8] E. Yoo, J. Kim, E. Hosono, H.S. Zhou, T. Kudo, I. Honma, Large Reversible Li Storage of Graphene Nanosheet Families for Use in Rechargeable Lithium Ion Batteries, Nano Lett. 8 (2008) 2277-2282.

[9] J. Xiao, D. Mei, X. Li, W. Xu, D. Wang, G.L. Graff, W.D. Bennett, Z. Nie, L.V. Saraf, I.A. Aksay, J. Liu and J.G. Zhang, Hierarchically Porous Graphene as a Lithium-Air Battery Electrode, Nano Lett. 11 (2011) 5071-5078.

[10] B. Seger, P.V. Kamat, Electrocatalytically Active Graphene-Platinum Nanocomposites. Role of 2-D Carbon Support in PEM Fuel Cells, J. Phys. Chem. C 113 (2009) 7990-7995.

[11] R. Kou, Y.Y. Shao, D.H. Wang, M.H. Engelhard, J.H. Kwak, J. Wang, V.V. Viswanathan, C.M. Wang, Y.H. Lin, Y. Wang, I.A. Aksay, J. Liu, Enhanced activity and stability of Pt catalysts on functionalized graphene sheets for electrocatalytic oxygen reduction, Electrochem. Commun. 11 (2009) 954-957.

[12] X. Wang, L.J. Zhi, N. Tsao, Z. Tomovic, J.L. Li, K. Mullen, Transparent Carbon Films as Electrodes in Organic Solar Cells, Angew. Chem.-Int. Ed. 47 (2008) 2990-2992.

ACCEPTED MANUSCRIPT

[13] J.B. Wu, H.A. Becerril, Z.N. Bao, Z.F. Liu, Y.S. Chen, P. Peumans, Organic Solar Cells with Solution-Processed Graphene Transparent Electrodes, Appl. Phys. Lett. 92 (2008) 263302-263303.

[14] S.J. Guo and S.J. Dong, Graphene and its derivative-based sensing materials for analytical devices, J. Mater. Chem. 21 (2011) 18503-18516.

[15] X.Y. Yang, X.Y. Zhang, Y.F. Ma, Y. Huang, Y.S. Wang and Y.S. Chen, Superparamagnetic graphene oxide–Fe_3O_4 nanoparticles hybrid for controlled targeted drug carriers, J. Mater. Chem. 19 (2009) 2710-2714.

[16] Y. Wang, S. Zhang, D. Du, Y.Y. Shao, Z.H. Li, J. Wang, M.H. Engelhard, J.H. Li and Y.H. Lin, Self assembly of acetylcholinesterase on a gold nanoparticles-graphene nanosheet hybrid for organophosphate pesticide detection using polyelectrolyte as a linker, J. Mater. Chem. 21 (2011) 5319-5325.

[17] J.D. Qiu, J. Huang, R.P. Liang, Nanocomposite film based on graphene oxide for high performance flexible, glucose biosensor, Sens. Actuators, B 160 (2011) 287-294.

[18] S.S. Han, H. Kim and N. Park, Effect of Shuttling Catalyst on the Migration of Hydrogen Adatoms: A Strategy for the Facile Hydrogenation of Graphene, J. Phys. Chem. C 115 (2011) 24696-24701.

[19] R.F. Nie, J.H. Wang, L.N. Wang, Y. Qin, P. Chen and Z.Y. Hou, Platinum supported on reduced graphene oxide as a catalyst for hydrogenation of nitroarenes, Carbon 50 (2012) 586-596.

[20] S. Stankovich, D.A. Dikin, G.H.B. Dommett, K.M. Kohlhaas, E.J. Zimney, E.A. Stach, R.D. Piner, S.T. Nguyen, R.S. Ruoff, Graphene-based composite materials, Nature 442 (2006) 282-286.

[21] D. Li, R.B. Kaner, Graphene-Based Materials, Science 320 (2008) 1170-1171.

[22] Q.L. Sheng, M.Z. Wang, J.B. Zheng, A novel hydrogen peroxide biosensor based on enzymatically induced deposition of polyaniline on the functionalized graphene-carbon nanotube hybrid materials, Sens. Actuators, B 160 (2011) 1070-1077.

[23] D. Zheng, S.K. Vashist, K. Al-Rubeaan, J.H.T. Luong, F.S. Sheu, Mediatorless amperometric glucose biosensing using 3-aminopropyltriethoxysilane-functionalized graphene, Talanta 99 (2012) 22-28.

[24] P.V. Kamat, Graphene-Based Nanoarchitectures. Anchoring Semiconductor and Metal Nanoparticles on a Two-Dimensional Carbon Support, J. Phys. Chem. Lett. 1(2010) 520-527.

[25] R. Muszynski, B. Seger, P.V. Kamat, Decorating Graphene Sheets with Gold Nanoparticles, J.

ACCEPTED MANUSCRIPT

Phys. Chem. C 112 (2008) 5263-5266.

[26] F. Cui, X.L. Zhang, Electrochemical sensor for epinephrine based on a glassy carbon electrode modified with graphene/gold nanocomposites, J. Electroanal. Chem. 669 (2012) 35-41.

[27] X.Q. Tian, C.M. Cheng, H.Y. Yuan, Simultaneous determination of L-ascorbic acid, dopamine and uric acid with gold nanoparticles-β-cyclodextrin–graphene-modified electrode by square wave Voltammetry, Talanta 93 (2012) 79-85.

[28] X.W. Liu, J.J. Mao, P.D. Liu, X.W. Wei, Fabrication of metal-graphene hybrid materials by electroless deposition, Carbon 49 (2011) 477-483.

[29] W. S. Hummers, R. E. Offeman, Preparation of Graphitic Oxide, J. Am. Chem. Soc. 80 (1958) 1339-1339.

[30] X.M. Sun, Z. Liu, K. Welsher, J.T. Robinson, A. Goodwin, S. Zaric and H.J. Dai, Nano-Graphene Oxide for Cellular Imaging and Drug Delivery, Nano Res. 1 (2008) 203-212.

[31] S. Stankovich, D.A. Dikin, R.D. Piner, Synthesis of graphene-based nanosheets via chemical reduction of exfoliated graphite oxide, Carbon 45 (2007) 1558-1565.

[32] Y.J. Li, W. Gao, L.J. Ci, C.M. Wang, P.M. Ajayan, Catalytic performance of Pt nanoparticles on reduced graphene oxide for methanol electro-oxidation, Carbon 48 (2010) 1124-1130.

[33] T. Liu, H.C. Su, X.J. Qu, P. Ju, L. Cui, S.Y. Ai, Acetylcholinesterase biosensor based on 3-carboxyphenylboronic acid/reduced graphene oxide-gold nanocomposites modified electrode for amperometric detection of organophosphorus and carbamate pesticides, Sens. Actuators, B 160 (2011) 1255-1261.

[34] K. Wang, Q. Liu, L.N. Dai, J.J. Yan, C. Ju, B.J. Qiu, X.Y. Wu, A highly sensitive and rapid organophosphate biosensor based on enhancement of CdS-decorated graphene nanocomposite, Anal. Chim. Acta 695 (2011) 84-88.

[35] S. Wu, X.Q. Lan, W. Zhao, Y.P. Li, L.H. Zhang, H.N. Wang, M. Han, S.Y. Tao, Controlled immobilization of acetylcholinesterase on improved hydrophobic gold nanoparticle/prussian blue modified surface for ultra-trace organophosphate pesticide detection, Biosens. Bioelectron. 27 (2011) 82-87.

[36] H.N Guan, F.L Zhang, J. Yu, D.F. Chi, The novel acetylcholinesterase biosensors based on liposome bioreactors-chitosan nanocomposite film for detection of organophosphates pesticides, Food Res. Int. 49 (2012) 15-21.

ACCEPTED MANUSCRIPT

[37] J.M. Gong, Z.Q. Guan, D.D. Song, Biosensor based on acetylcholinesterase immobilized onto layered double hydroxides for flow injection/amperometric detection of organophosphate pesticides, Biosens. Bioelectron. 39 (2013) 320-323.

[38] R. Xue, T.F. Kang, L.P. Lu, S.Y. Cheng, Immobilization of acetylcholinesterase via biocompatible interface of silk fibroin for detection of organophosphate and carbamate pesticides, Appl. Surf. Sci. 258 (2012) 6040-6045.

[39] S. Viswanathan, H. Radecka, J. Radecki, Electrochemical biosensor for pesticides based on acetylcholinesterase immobilized on polyaniline deposited on vertically assembled carbon nanotubes wrapped with ssDNA, Biosens. Bioelectron. 24 (2009) 2772-2777.

[40] Y.H. Qu, Q. Sun, F. Xiao, G.Y. Shi, L.T. Jin, Layer-by-Layer self-assembled acetylcholinesterase/PAMAM-Au on CNTs modified electrode for sensing pesticides, Bioelectrochemistry 77 (2010) 139-144.

[41] G. Silva Nunes, G. Jeanty, J.L. Marty, Enzyme immobilization procedures on screen-printed electrodes used for the detection of anticholinesterase pesticides Comparative study, Anal. Chim. Acta 523 (2004) 107-115.

ACCEPTED MANUSCRIPT

ACCEPTED MANUSCRIPT

Footnotes:

1 Abbreviations used: CGR, carboxylic graphene; GO, graphene oxide; NP, nanoparticle; Pt, platinum; NF, nafion; CS, Chitosan; ATCl ,acetylthiocholine chloride; AChE, acetylcholinesterase; GCE, glassy carbon electrode; PBS, phosphate-buffered saline; SEM, scanning electron microscopy; FTIR, Fourier transform infrared spectrometry; UV–vis, UV–vis absorption spectroscopy; CV, cyclic voltammetry; RSD, relative standard deviation; DI, deionized; K_m^{app}, apparent Michaelis–Menten constant;

ACCEPTED MANUSCRIPT

Figure Captions:

Fig. 1 SEM images of GO (a), CGR (b) and Pt NPs-CGR (c).

Fig. 2 (A) FTIR spectra image of GO (a) and CGR (b); (B) UV–vis absorption spectra of PtNPs solution synthesized in the absence (a) and presence (b) of CGR.

Fig. 3 (A) CV of NF/AChE-CS/GCE (a), NF/AChE-CS/GO-NF/GCE (b), NF/AChE-CS/CGR-NF/GCE (c), NF/AChE-CS/PtNPs-CGR-NF/GCE (d) in 0.1M pH 7.4 PBS and NF/AChE-CS/GCE (e), NF/AChE-CS/GO-NF/GCE (f), NF/AChE-CS/CGR-NF/GCE (g), NF/AChE-CS/PtNPs-CGR-NF/GCE (h) in 0.1M pH 7.4 PBS containning 0.5 mM ATCl. Scan rate: 0.10V/s in 25℃; (B) Amperometric response of the NF/AChE-CS/PtNPs-CGR-NF/GCE (a), AChE-CS/PtNPs-CGR-NF/GCE (b) and AChE/PtNPs-CGR- NF/GCE (c) for six assays.

Fig. 4 (A) Typical current–time plot for the sensor on successive addition of stock ATCl to pH 7.4 PBS, insets show the calibration curves for ATCl determination; (B) Calibration plot for the ATCl sensor, inset shows the Lineweaver–Burk plot of $1/i_{ss}$ vs. $1/C$.

Fig. 5 (A) CV of the NF/AChE-CS/PtNPs-CGR-NF/GCE in pH 7.4 PBS containing 0.5mM ATCl after incubation with 0 (a), 10^{-13}M (b), 10^{-11}M and (c) 10^{-9}M (b) methyl parathion for 6 min; (B) Inhibition curves of NF/AChE-CS/PtNPs-CGR-NF/GCE biosensor for methyl parathion (a) and carbofuran (b) determination after 6-min incubation.

Figure (1)

ACCEPTED MANUSCRIPT

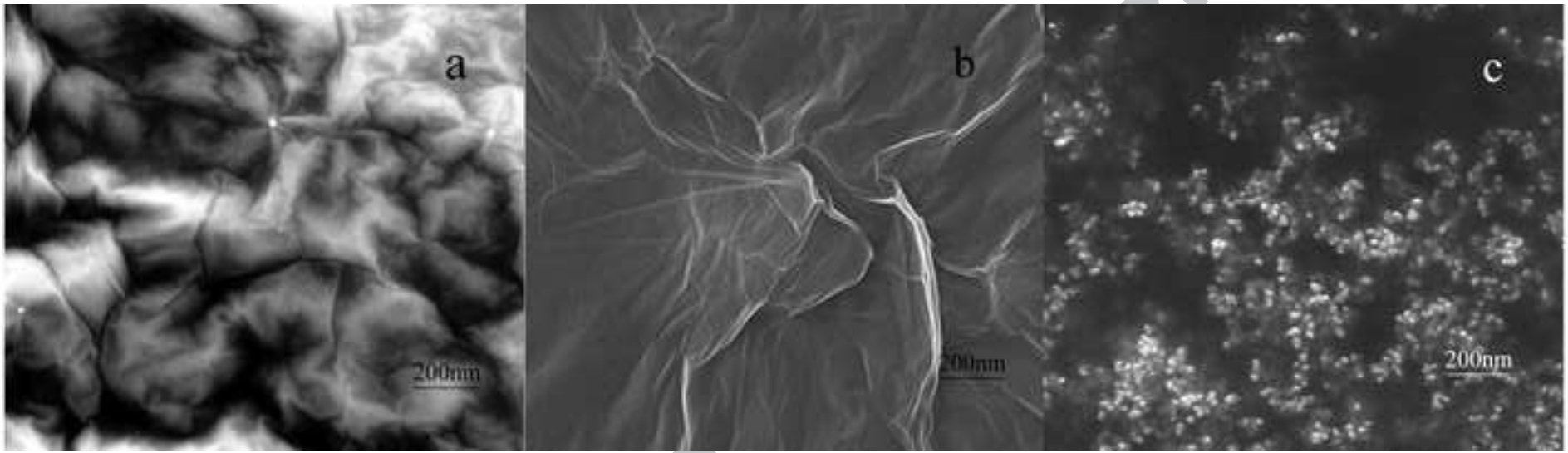

ACCEPTED MANUSCRIPT

Figure (2)

ACCEPTED MANUSCRIPT

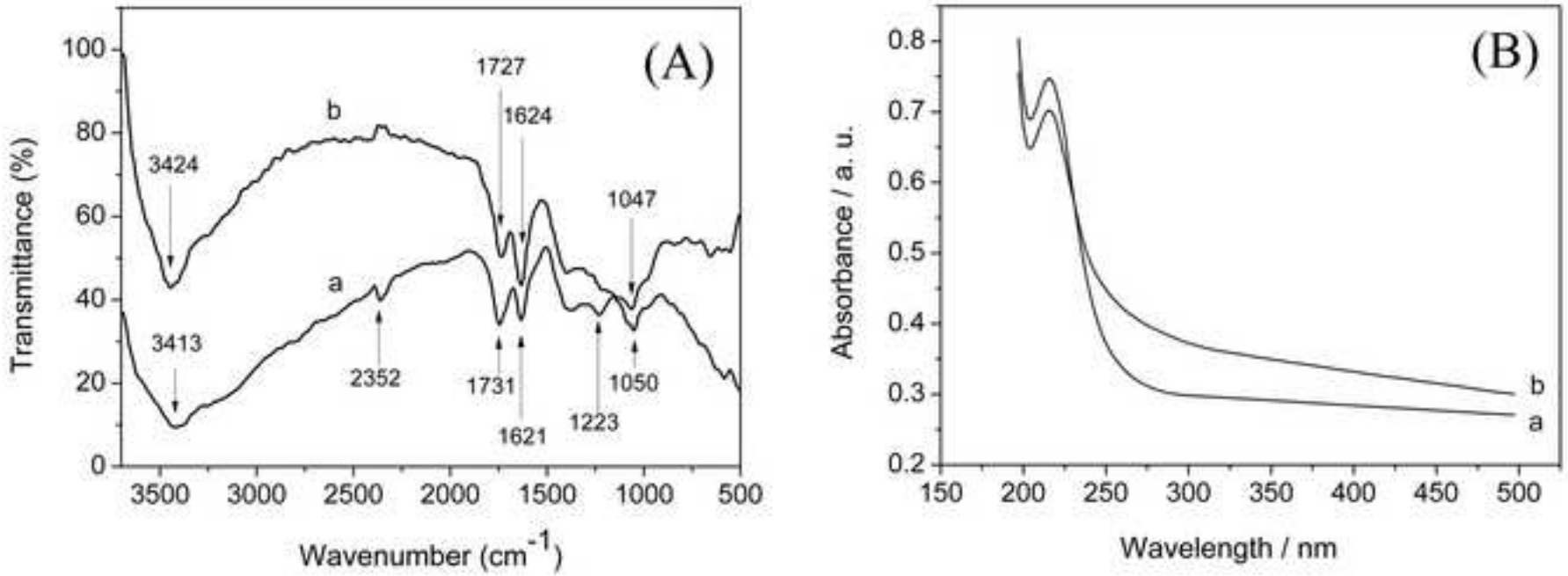

ACCEPTED

Figure (3)

ACCEPTED MANUSCRIPT

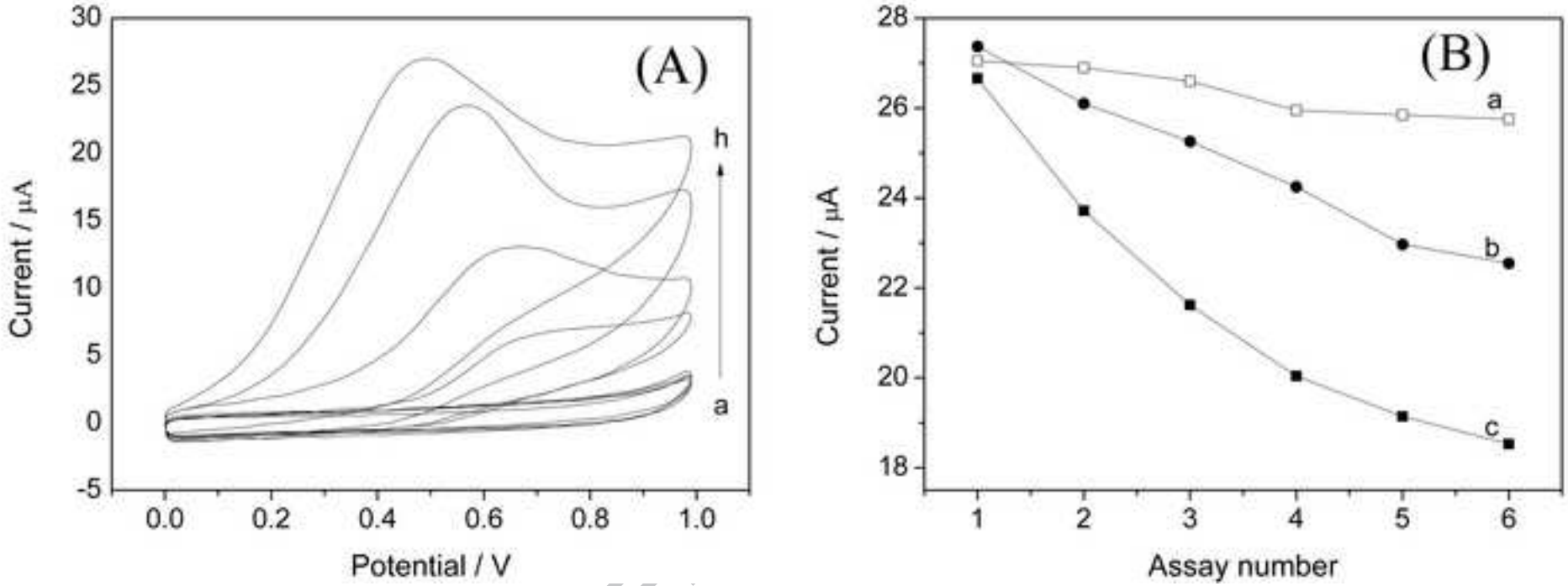

ACCEPTED

Figure (4)

ACCEPTED MANUSCRIPT

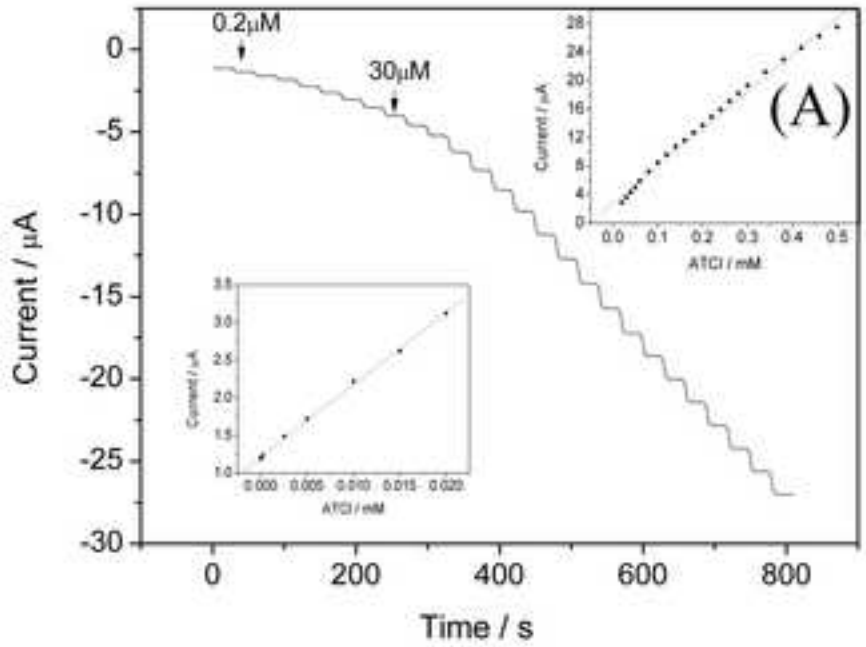

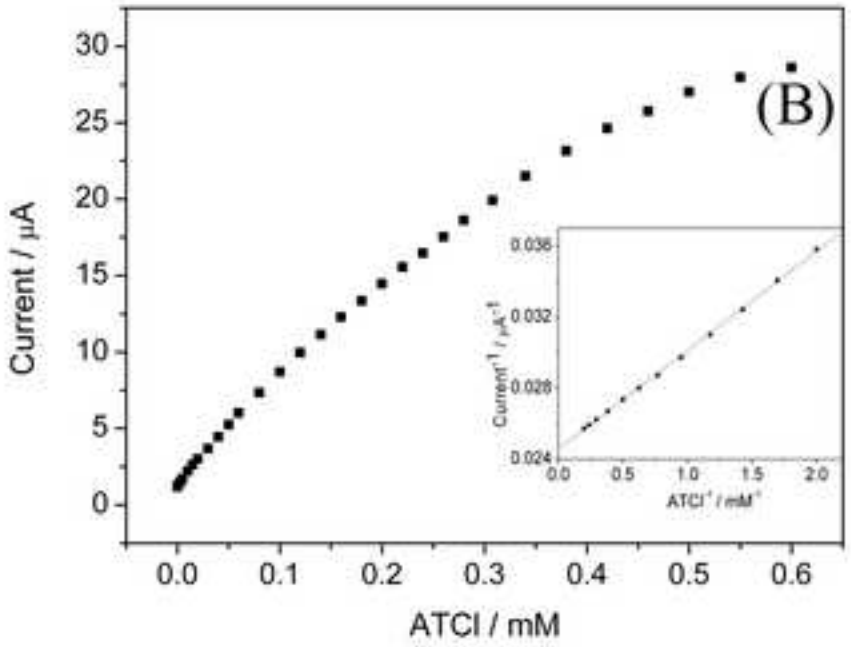

ACCEPTED

Figure (5)

ACCEPTED MANUSCRIPT

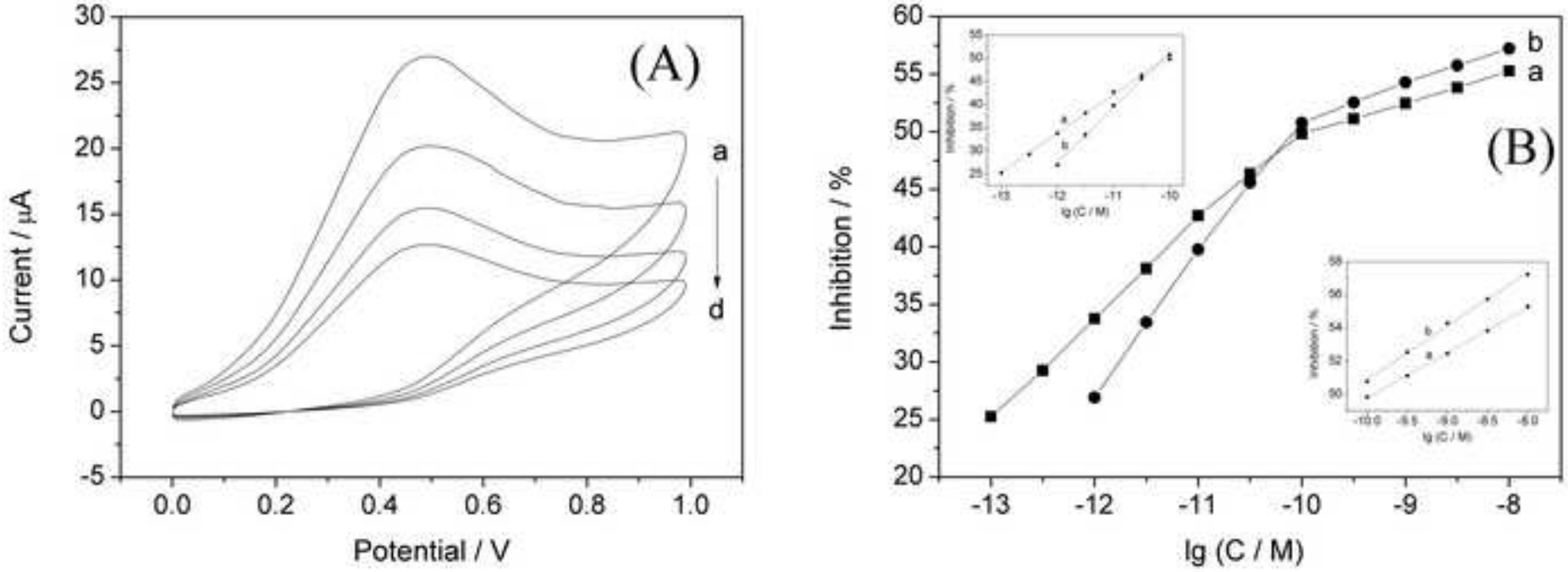

ACCEPTED

ACCEPTED MANUSCRIPT

Table 1

Comparison of the response of the biosensor for detection of pesticides with other biosensor based on immobilized AChE.

Sample	Electrode	Liner range (M)	Detection limit (M)	References
methyl parathion	AChE-LDHs[a]/GCE	1.9×10^{-8}-1.1×10^{-6}; 1.1×10^{-6}- 1.5×10^{-5}	2.3×10^{-9}	[37]
	AChE-SF[b]/MWNTs[c]/GCE	3.5×10^{-6} - 2.0×10^{-3}	5.0×10^{-7}	[38]
	Au[d]/ssDNA[e]-SWCNT/PANI[f]/AChE	1.0×10^{-11} - 1.0×10^{-6}	1.0×10^{-12}	[39]
	NF/AChE-CS/PtNPs-CGR-NF/GCE	10^{-13} - 10^{-10}; 10^{-10}- 10^{-8}	5.0×10^{-14}	This work
Carbofuran	AChE/PAMAM[g]-Au/CNTs/GCE	4.5×10^{-9}- 9.0×10^{-8}	4.0×10^{-9}	[40]
	AChE-TCNQ[h]/SPE[i]	9.0×10^{-10}- 7.5×10^{-7}	9.0×10^{-10}	[41]
	NF/AChE-CS/PtNPs-CGR-NF/GCE	10^{-12} - 10^{-10}; 10^{-10}- 10^{-8}	5.0×10^{-13}	This work

a. Layered double hydroxides.

b. Silk fibroin.

c. Multiwalled carbon nanotube.

d. Gold electrode.

e. Single strand oligonucleotide.

f. Polyaniline.

g: Polyamidoamine.

h: 7,7,8,8-tetracyanoquinodimethane.

i: Screen-printed electrode.